

Spin-Wave Phenomena in Liquid ^3He Systems*

L. R. Corruccini,† D. D. Osheroff,† D. M. Lee, and R. C. Richardson

Laboratory of Atomic and Solid State Physics, Cornell University, Ithaca, New York

(Received January 3, 1972)

The magnetic effects predicted by Leggett and Rice for Fermi liquids in the collisionless regime have been verified. Spin-echo measurements are reported which demonstrate the existence of spin waves and undamped spin currents in liquid ^3He and dilute ^3He - ^4He solutions. The experimental results are compared with the theoretical expressions of Leggett and Rice, and values of the Fermi liquid interaction parameter

$$\lambda = [I/(I + F_0^a)] - \{I/[I + (F_1^a/3)]\}$$

are derived for three samples: liquid ^3He at $P = 0$ and 27 atm, and a 6.4% ^3He - ^4He solution. In addition, some techniques for direct observation of individual spin-wave modes are explored and the results reported.

1. INTRODUCTION

Among the many unusual low-temperature properties of liquid ^3He , one of the most unique is the category of collisionless wave phenomena. First predicted by L. D. Landau¹ in 1956, these are wave disturbances which propagate only in the absence of quasiparticle collisions, when the condition $\omega\tau \gg 1$ holds. Here, ω is the frequency of the wave disturbance, and τ is the fermion collision relaxation time, proportional to $1/T^2$. Landau's predictions fall into two categories—zero sound and spin waves. The first of these is associated with a spin-independent oscillatory perturbation of the Fermi sphere, and was verified experimentally by Abel *et al.*² in 1966. The second corresponds to an antisymmetric oscillation of the Fermi sphere, and is the topic of this paper.

*Work supported in part by the National Science Foundation through Grant No. GP-24179 and the Advanced Research Projects Agency through the Cornell Materials Science Center, Report No. 1698.

†National Science Foundation Predoctoral Fellow.

It was noted by Landau that spin waves would not propagate in ^3He in zero magnetic field, due to the negative exchange interaction between ^3He spins. Subsequent inclusion of a magnetic field in the Fermi liquid kinetic equation by Silin³ and Platzman and Wolff⁴ showed that spin waves would propagate in finite fields with an altered dispersion relation. Dispersion diagrams for ^3He and dilute ^3He - ^4He solutions are shown in Fig. 1. The effect of the magnetic field is to "pull" the spin-wave curve for small k away from the shaded single-quasiparticle excitation continuum, making observation of the spin waves possible in this region.

Platzman and Wolff derived an expression for the dynamic susceptibility $\chi(k, \omega)$ for Fermi liquids, which exhibits directly the presence of spin-wave modes. In the long-wavelength limit, it is given by

$$\chi(k, \omega) = (-m^*/m)\chi_0\Omega_0/(\omega - \omega_0 + iD^*k^2) \quad (1)$$

where

$$D^* = (1/3)[(v_F^2(1 + F_0^a)\tau_D)/(i\omega_0\lambda\tau_D + 1)]$$

and

$$\lambda = [1/(1 + F_0^a)] - \{1/[1 - (F_1^a/3)]\}$$

Here, χ_0 is the static susceptibility of an ideal Fermi gas, $\omega_0/2\pi$ is the Larmor frequency, k is the spin-wave wave vector, F_0^a and F_1^a are conventional Fermi liquid interaction parameters, $\Omega_0 = \omega_0/(1 + F_0^a)$, v_F is the Fermi velocity, τ_D is the spin diffusion relaxation time,⁵ and m^* is the effective mass. At high temperatures or small Larmor frequencies the coefficient D^* reduces to a real number, the spin diffusion coefficient. Spin disturbances

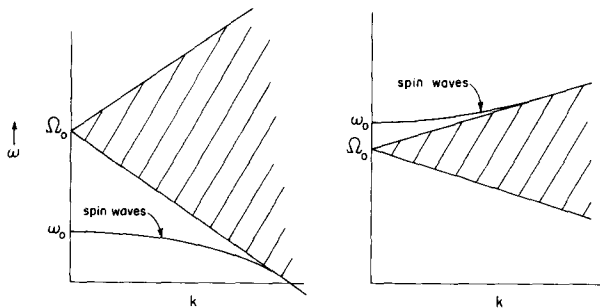


Fig. 1. Spin-wave dispersion curves in a magnetic field. At left is the spectrum for ^3He at $P = 0$. At right, that for dilute ^3He - ^4He solutions (not to scale). The shaded region is the spectrum for spin-flip excitations of single quasiparticles above the Fermi surface. Only F_0^a has been used in calculating the spin-wave curves.

propagate diffusively rather than as waves. The term iD^*k^2 contributes a diffusional broadening to the single pole of $\chi(k, \omega)$ at ω_0 , the Larmor resonance. In the opposite limit $\omega_0\lambda\tau_D \gg 1$, the "collisionless regime," D^* becomes imaginary, and $\chi(k, \omega)$ exhibits a new family of poles for finite k . These are the spin waves.

Unfortunately an NMR measurement of $\chi(k, \omega)$ requires an oscillatory exciting field which varies spatially on the scale of the spin-wave wavelength. This is difficult to achieve in the case of liquid ^3He , because a k of about 10^3 cm^{-1} or greater is necessary to separate spin wave from Larmor resonance in (1). In the analogous case of electrons in alkali metals the experimental situation is made easier owing to the electrons' charge, and spin-wave poles have been observed using CESR techniques.⁶

In 1968 Leggett and Rice⁷ provided a second and more accessible test for the presence of spin waves in ^3He . They describe a variation of the usual spin-echo technique to measure directly the real part of the complex diffusion coefficient D^* . The standard theory of spin echoes⁸ assumes that the nuclear spin magnetization $M(r, t)$ obeys the classical diffusion equation

$$D\nabla^2 M + (\partial M/\partial t) + \gamma(M \times H) = 0 \quad (2)$$

from which the attenuation of each spin echo relative to the previous one is given by

$$E = \exp\left(-\frac{1}{2}D\gamma^2 G^2 t_0^2\right) \quad (3)$$

where t_0 is the time interval between the two echoes, γ is the gyromagnetic ratio, and G is an applied magnetic field gradient. By measuring experimentally the logarithmic decrement of successive echoes as a function of t_0 or G , D may be obtained. The spin diffusion coefficient defined by (2) has been calculated for Fermi liquids by Hone⁵ with the result

$$D_0 = \frac{1}{3}v_F^2(1 + F_0^a)\tau_D \quad (4)$$

1.1. The Leggett-Rice Effect

In a series of papers Leggett and Rice⁷ and Leggett^{9,10} show that the assumption of (2) is incorrect when $\omega\tau_D \gtrsim 1$. Instead, assuming "hydrodynamic" conditions (see Ref. 10), the magnetization M and spin current J are coupled in an unusual nonlinear fashion as shown below:

$$\mathbf{M} + \nabla \cdot \mathbf{J} - \gamma \mathbf{M} \times \mathbf{H} = 0 \quad (5)$$

$$\begin{aligned} \dot{\mathbf{J}} + (V_F^2/3)[1 + F_0^a][1 + (F_1^a/3)]\nabla \mathbf{M} - \gamma \mathbf{J} \times \mathbf{H} \\ + [\hbar(dn/d\varepsilon)]^{-1}[F_0^a - (F_1^a/3)]\mathbf{J} \times \mathbf{M} = (\partial \mathbf{J}/\partial t)_{\text{coll}}. \end{aligned} \quad (6)$$

The new feature of these equations is the term $\mathbf{J} \times \mathbf{M}$ in (6). Ordinarily this term is negligible, since if $(\partial\mathbf{J}/\partial t)_{\text{coll}}$ is assumed proportional to $1/\tau_D$ then J will relax in a time short compared with one Larmor rotation $1/\omega_0$. Equations (5) and (6) then reduce to (2). In the collisionless regime $\omega\tau > 1$ this term cannot be ignored, however; it says J exerts a torque on M even in the locally rotating frame. It will be seen that this nonlinear effect will be maximal if M is rotated perpendicular to the external field H_0 . The field gradient G causes M to twist up in a spiral along H_0 , creating a magnetization gradient ∇M which is perpendicular to M and proportional to $|M^+| = M \sin \phi$. For $\phi = 90^\circ$, ∇M drives large spin currents parallel to itself, and H_0 , M , and J are all mutually perpendicular, maximizing $\mathbf{J} \times \mathbf{M}$. This is the situation created by a "90°" NMR pulse.

When specialized to the case of a typical spin-echo experiment, in which M is rotated by an angle ϕ with respect to the external field H_0 by an initial pulse and then followed at times $t_0/2, 3t_0/2, 5t_0/2, \dots$, by an equally spaced series of 180° pulses, the echo amplitudes predicted by (5) and (6) at $t_0, 2t_0, 3t_0, \dots$, are given by

$$\ln h_n - \delta(1 - h_n)^2 = -(n/12)[D_0(\gamma G)^2 t_0^3 / (1 + \alpha^2 \cos^2 \phi)] \quad (7)$$

Here

$$\begin{aligned} \alpha &= \lambda \omega_0 \tau_D \\ \lambda &= [1/(1 + F_0^a)] - [1/(1 + F_1^a/3)] \\ \delta &= (\alpha^2/2) \sin^2 \phi / (1 + \alpha^2 \cos^2 \phi) \end{aligned}$$

where h_n is the height of the n th echo relative to its height at $G = 0$ or $t = 0$, and D_0 is Hone's result (4) for D .

As can be seen, the echo envelope is no longer exponential. As outlined above, the nonexponential behavior is maximal for $\phi = 90^\circ$ due to large undamped spin currents. In the opposite limit $\sin \phi \rightarrow 0$, ∇M is small and spin currents are only weakly excited. As seen from (7) the echo envelope becomes exponential, agreeing with the standard result (3) if D is replaced by

$$D_{\text{eff}} = D_0 / (1 + \alpha^2 \cos^2 \phi) \quad (8)$$

A closer look shows that this D_{eff} is just the real part of the complex D^* in the spin-wave susceptibility (1), with an additional $\cos^2 \phi$ dependence in the denominator. For constant ϕ , the D_{eff} exhibits a maximum as a function of temperature, in contrast to D_0 at low fields, which is proportional to $1/T^2$. By varying T or ϕ a direct measure of the interaction parameter λ may be obtained, giving a value for the hitherto unmeasured F_1^a .

In view of the similarity between D_{eff} and the spin-wave dispersion coefficient D^* it is natural to ask whether the Leggett-Rice effect involves the

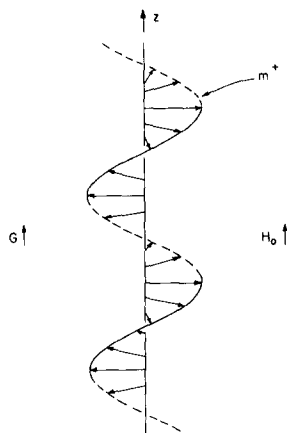


Fig. 2. Spin-wave excitation mechanism. The gradient G causes m^+ to twist up along H_0 , as observed from the reference frame rotating with frequency ω_0 . The spatially periodic magnetization excites spin waves with matching wave vector k .

excitation of spin-wave modes. The answer is certainly yes,¹¹ and the mechanism by which the spin-waves are generated is shown in Fig. 2. In the presence of the gradient G , the precessing magnetization m^+ twists up along the z direction, the spatially nonuniform magnetization generating wave components for which $k \neq 0$. Since the pitch of the magnetization helix constantly increases, the generation is broadband, exciting spin waves of all wavelengths in the long-wavelength region.

From these arguments it will be seen that the Leggett-Rice effect involves two separate phenomena, undamped spin currents in the limit $\sin \phi \rightarrow 1$, and spin waves in the limit $\sin \phi \rightarrow 0$. The purpose of this paper is to report a detailed verification of both limits as embodied in Eq. (7). Measurements are reported on pure ^3He at $P = 0$ and 27.0 atm, and on a dilute ^3He - ^4He mixture of 6.4% at $P = 0$. Values of the interaction parameter λ are extracted for all three. Preliminary results for ^3He at $P = 0$ have been described by us in a previous letter.¹² In addition, some techniques for observation of spin-wave poles in $\chi(k, \omega)$ are explored and the results reported.

2. EXPERIMENTAL APPARATUS AND PROCEDURE

2.1. Cryostat

The high magnetic fields and very low temperatures necessary to observe spin-wave effects place special requirements on the experimental cooling apparatus. Adiabatic demagnetization is cumbersome in the presence of large fields, and single-shot dilution refrigeration provides rather limited cooling capacity at these temperatures. Cooling for the measurements to be described was provided by a dilution refrigerator in tandem with a

"Pomeranchuk effect" ^3He compressional cell. This arrangement has the advantages of compactness and essentially field-independent cooling capacity. In the millidegree temperature range, compressional cooling is capable of removing an order of magnitude more heat per unit volume of ^3He than single-shot dilution refrigeration.

The principles of the dilution cooling process and the Pomeranchuk effect are by now well known, and the reader is referred to Refs. 13, 14, and 15 for detailed information. The distinguishing feature of the present apparatus is the epoxy sample chamber, which is attached to the compressional cell and linked to it thermally by a wire brush containing 17 g of No. 52 AWG copper wire. This arrangement cooled approximately 2 cm^3 of sample to 5 or 6 mK in fields up to 14 kG. The apparatus is shown in Fig. 3.

Compression of the ^3He in the Pomeranchuk cell was performed by the two beryllium copper bellows labeled in Fig. 3. They act as a pressure transformer. The upper bellows is filled with pressurized ^4He , forcing the

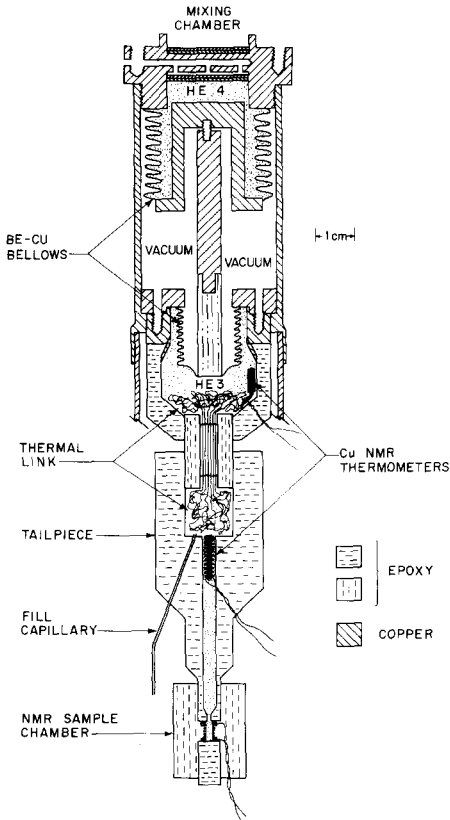


Fig. 3. Cooling apparatus and sample cell. The flange at the top of the apparatus forms the bottom of the dilution refrigerator mixing chamber. The upper metal bellows is forced downward by pressurized ^4He , compressing liquid ^3He in the cell below via the connecting rod and smaller bellows. The resulting adiabatic solidification of the ^3He cools the sample in the tailpiece below through the brush of copper wires labeled Thermal Link.

smaller ^3He bellows downward via the connecting rod. The ratio of cross-sectional areas for the two bellows is approximately 3.5:1, meaning that the ^3He may be completely solidified without raising the ^4He pressure above 10 atm. Thermal isolation from the mixing chamber during compressions is provided by the Kapitza thermal boundary resistance between ^3He and chamber walls.

For pulsed NMR measurements at these temperatures eddy-current heating becomes a problem. The NMR coil, which acted both as transmitter and receiver, was therefore placed at the bottom of an epoxy tailpiece containing a 3.18-mm-diam connecting hole, removing it 3.3 cm from the thermometer and wire brush and 7.6 cm from the metal parts of the Pomeranchuk cell above. The small diameter of the coil, 1.7 mm, was chosen both for high-frequency tuning and to minimize fringing rf fields.

The NMR sample chamber and tailpiece were made from the epoxy Stycast 1269A, manufactured by Emerson and Cuming, Inc., Canton, Massachusetts. It has negligible magnetic properties and is nearly as tough as Epibond 100A, the standard low-temperature epoxy; in addition it is transparent. The sample chamber was made simply by close winding with small end corrections a coil of number 32 AWG 99.999% Cu wire over a piece of 1.7-mm-o.d. Teflon spaghetti strengthened with a steel rod, and casting it in a Teflon mold. With the spaghetti removed and the ends counter-bored and plugged, the coil is 4.6 mm long and has a filling factor close to 100%.

The compression cell was made by machining a Teflon plug with the desired shape for the inside of the cell, inserting it into a copper flange with a feathered collar along with a little fast-curing epoxy to make a seal, and allowing the assembly to harden. The piece was then suspended in a transparent nalgene mold, which was filled with epoxy up to the flange. The chamber used in these experiments was made of Stycast 1266, a room-temperature cure variant of Stycast 1269A. The transparency of the epoxy makes it possible to see bubbles and other defects in the casting while there is time to rectify them. After curing, the Teflon plug is machined out.

The wire brush was made by pulling 17 g of No. 52 AWG copper wires (Formex insulated) through a 1.3-cm-diam cylinder of Stycast 1266 with a center hole 6.4 mm in diameter. A vacuum-tight seal was made by injecting a small amount of partially cured epoxy into the middle of the hole with a hypodermic needle. The epoxy had to be quite viscous to prevent creeping by capillary action into the free ends of the brush.¹⁶ Holes were bored into the bottom of the compression cell and the top of the connecting tailpiece, and the cylinder sealed into place with Stycast 1266. To minimize the volume of sample to be cooled, the lower end of the brush was pressed into the tailpiece using the tailstock of a large lathe.

When completed, the compression cell ﬂange was bolted to the ^3He bellows assembly with a 0.38-mm-diam lead O-ring seal. Electrical connections to the NMR coil were made with coaxial cable assembled from 0.99-mm-o.d. \times 0.74-mm-i.d. stainless-steel capillary tubing, No. 32 teflon spaghetti, and 0.08-mm-diam 50% Mo–Re superconducting center conductor. The Mo–Re wire was obtained from Bridgeport Insulated Wire Company, Bridgeport, Connecticut. This coax is thermally grounded at the final refrigerator heat exchanger, and extends up to the 4 K exchange gas ﬂange, where it is again thermally grounded. From this ﬂange up to the top of the cryostat, commercial “Micro Coax” with 1.0-mm-o.d. stainless-steel outer conductor and copperweld center conductor is used.

The ﬁlling capillary for the sample chamber was 0.1-mm-i.d. \times 0.4-mm-o.d. copper–nickel tubing. The small i.d. was chosen partly to minimize heat leaks from warmer parts of the cryostat, and also to minimize concentration changes in the ^3He – ^4He mixtures caused by the thermomechanical effect. It was thermally grounded to the still and final heat exchanger of the dilution refrigerator. All capillary tubing used in the cryostat construction, as well as the “Micro Coax,” was obtained from Uniform Tubes, Inc., Collegeville, Pennsylvania. Handling of the gaseous samples, as well as the ^3He for the compression cell, was facilitated by high-pressure “dip sticks” with activated charcoal adsorbent. When inserted into a standard 50-liter ^4He storage Dewar, they would remove up to 2 cm³ of liquid He sample at 4 K through 0.1-mm-i.d. capillaries in a few hours.

During a typical experimental run, the compressional cell was ﬁrst pressurized to 29.5 atm with ^3He . The apparatus was then cooled to 25–30 mK by the dilution refrigerator, forming a solid ^3He block in the ﬁll capillary at a temperature in the vicinity of the melting-curve minimum at $T = 0.3$ K. Compression of the ^3He in the Pomeranchuk cell was begun by slowly raising the pressure in the ^4He bellows, using a high-pressure ^4He cylinder with a needle valve throttle. Compressions took from 8 to 12 h, in order to maintain thermal equilibrium and maximize cooling eﬃciency between the ^3He cell and experimental chamber. The limiting low temperature was somewhat ﬁeld dependent; cooling progressed to about 4 mK in a 2.5-kG ﬁeld but was limited to about 6 mK at 11.3 kG. Corresponding ^3He compression cell temperatures were approximately 3 and 4.5 mK.

NMR measurements on the sample were generally taken while warming up, after waiting 15–30 min for thermal equilibrium. The sample chamber would remain at the lowest temperature for up to 4 h, then slowly warm up to 9 or 10 mK over a period of roughly 5 h. Further warming above 10 mK had to be produced by partial decompression of the ^3He cell. These long warmup times were a great advantage when making diﬀusion measurements, which tend to be time consuming, especially when small temperature increments between points are desired.

2.2. Thermometry

Thermometry in large fields presents a problem, since the usual paramagnetic salts cannot be used. For these experiments a cw NMR thermometer was used, which continually monitors the nuclear susceptibility $\chi''(\omega)$ of ^{63}Cu . The nuclear susceptibility of copper obeys Curie's law with negligible departures up to 15 kG. The thermometer itself is a 3-mm bundle of No. 52 AWG Formex insulated copper wire contained within a close-wound coil of No. 32 AWG copper wire approximately 1 cm long. The inductance of the coil was approximately $1 \mu\text{H}$. Two of these coils were used, one in the compression cell and one in the sample cell. Electrical connections were identical to those for the NMR coil.

A block diagram of the thermometer electronics is shown in Fig. 4. The rf oscillator is frequency modulated at 100 Hz while the magnet sweeps slowly through the ^{63}Cu Larmor resonance. The resulting signal from the phase-sensitive detector is roughly the derivative of $\chi''(\omega)$, and is inversely proportional to temperature.¹⁷ The magnet used for the experiment had 38-cm pole faces and a gap of 8.9 cm. When data points were taken the magnet sweep was turned off.

The thermometer was calibrated using the measured temperature dependence of the ^3He melting pressure.^{18*} The pressure was measured

* Values of the low temperature melting curve used in this work are those given in R. T. Johnson, O. V. Lounasmaa, R. Rosenbaum, O. G. Symko, and J. C. Wheatley, *J. Low Temp. Phys.* **2**, 403 (1970).

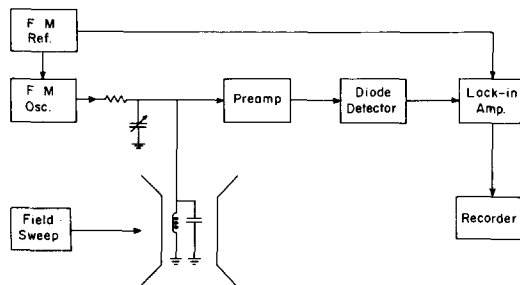


Fig. 4. Thermometer electronics. The cw oscillator is frequency modulated at 100 Hz as the magnetic field is swept back and forth through the ^{63}Cu resonance. The tank circuit rf level is rectified and detected by the lock-in amplifier, yielding a signal which is roughly the derivative of the nuclear susceptibility $\chi''(\omega)$. This signal amplitude is proportional to $1/T$.

using a cylindrical capacitor mounted on the rod connecting the two bellows, which measured the deflection of the ^3He bellows. Capacitance was calibrated as a function of differential pressure between ^3He and ^4He bellows, generally at 1 K before a run. Calibrations of ^{63}Cu susceptibility vs. T were made above 20 mK, where field-dependent corrections to the melting curve are negligible. Calibration points were taken after many thermal time constants to insure equilibrium between the compression cell and sample cell. Self-consistency between different calibration points was better than 5%.

Voltages applied across the thermometer coils did not exceed $30\ \mu\text{V}$, giving a signal-to-noise ratio of approximately 50 below 20 mK at low fields and over 100 at high fields. Power level checks indicated that errors due to saturation of the Larmor resonance and ohmic heating in the copper wires should be negligible above 2 mK.

2.3. Pulsed NMR Setup and Sequence of Measurements

The NMR spectrometer is of standard design^{19,20} except for the fact that it is transistorized throughout; 90° pulse lengths varied from $9\ \mu\text{sec}$ at 7.9 MHz to $80\ \mu\text{sec}$ at 36.7 MHz. The Maxwell coils²¹ used to provide the gradients for spin diffusion measurements were mounted between the magnet pole faces and the glass nitrogen Dewar. Current was measured with a digital ammeter. Gradients used in this experiment ranged from zero to $60\ \text{G/cm}$.

The gradient produced by these coils was calibrated as a function of current by measuring the null times on both sides of an echo as current was varied. For a cylindrical sample the echo decay envelope is proportional²² to $J_1(\gamma G dt/2)$, where J_1 is a first-order Bessel function, d is the sample diameter, γ is the gyromagnetic ratio, and t is the time. The gradient may be determined by observing the time at which the first Bessel function zero occurs: $J_1(3.83) = 0$. Calibrations were generally made using echoes rather than free-induction decays to eliminate errors due to oscilloscope triggering and the finite length of 90° pulses. The residual gradient at $I = 0$ was observed to be a few parts in 10^6 of H_0 across the 1.7-mm sample.

Measurements of echo amplitudes were taken as a function of field gradient alone. T_2 -type damping was present in both ^3He and ^3He - ^4He mixture measurements, and made comparison of time-sequence echo measurements with Leggett's Eq. (7) difficult. Typical times between the initial pulse and the first 180° pulse were 3 msec for ^3He and 0.5 msec, 1 msec, and 2 msec for mixtures. A General Radio type 1191 electronic counter-timer was used as a time standard for the pulse spacing. Within the scatter of experimental data, boundary-limited diffusion was not detectable in either ^3He or dilute mixture measurements.

3. SPIN DIFFUSION RESULTS AND DISCUSSION

3.1. Data Handling Procedure

Measurements of the diffusion coefficient, determined from the damping of spin echoes in a field gradient G , were made in various magnetic fields between 2.5 and 11.5 kG in the temperature range 35–5 mK. The results were compared with the theoretical expressions of Leggett and Rice using the following procedure. First the low-field (2.5 kG) data were analyzed using Hone's expression for D_0 [Eq. (4)]:

$$D_0 = (v_F^2/3)(1 + F_0^a)\tau_D$$

D_0 was obtained from the analysis of the ratio of echo amplitudes in the pulse sequence 90° – 180° – 180° . In this field the echo ratios obeyed the exponential attenuation law (3) at temperatures above about 10 mK in all samples studied. Using values of v_F and F_0^a determined by previous workers^{23–25} a value of τ_D was derived. Using this τ_D the high-field data was then analyzed.

According to Leggett's Eq. (7), in the limit of small initial pulse angle ϕ the echo amplitudes should obey an exponential attenuation law:

$$\ln h_n = -(1/12)[nD_0\gamma^2G^2t_0^3/(1 + \alpha^2 \cos^2\phi)] \quad (\text{small } \phi)$$

where $\alpha = \lambda\omega_0\tau_D$. This equation may easily be inverted to give λ in terms of h_n , G , and D_0 . Using the pulse sequence ϕ – 180° – 180° , where ϕ was always less than 20° , a value of λ for each echo height h_1 and h_2 in various gradients was obtained for temperatures lying below the peak in the effective diffusion coefficient, $D_e = D_0/(1 + \alpha^2 \cos^2\phi)$. The peak occurs at a temperature given by $1 = \alpha \cos \phi$. The resulting values of λ were weighted according to the relative sensitivity of D_e to λ at that temperature, or $(1/D)(\partial D_e/\partial \lambda)$, and averages and standard deviations computed. A recursive analysis for λ using the full equation (7) changes λ by less than 2%, much less than the experimental uncertainty.

Using the mean λ obtained by this procedure, low-temperature diffusion data were analyzed for a variety of initial pulse angles ϕ in the pulse sequence ϕ – 180° – 180° . Here the full echo attenuation equation was used [Eq. (7)]:

$$\ln h_n - \delta(1 - h_n^2) = -\frac{1}{12}[nD_0\gamma^2G^2t_0^3/(1 + \alpha^2 \cos^2\phi)]$$

The left-hand side of (10) was plotted vs. $(\gamma G)^2$, and $D_e(\phi)$ was determined from the slopes of straight lines drawn through the points.

3.2. ^3He at $P = 0$

Results for the effective diffusion coefficient D_e with an initial pulse angle ϕ of 18° are shown as a function of temperature in Fig. 5. The data

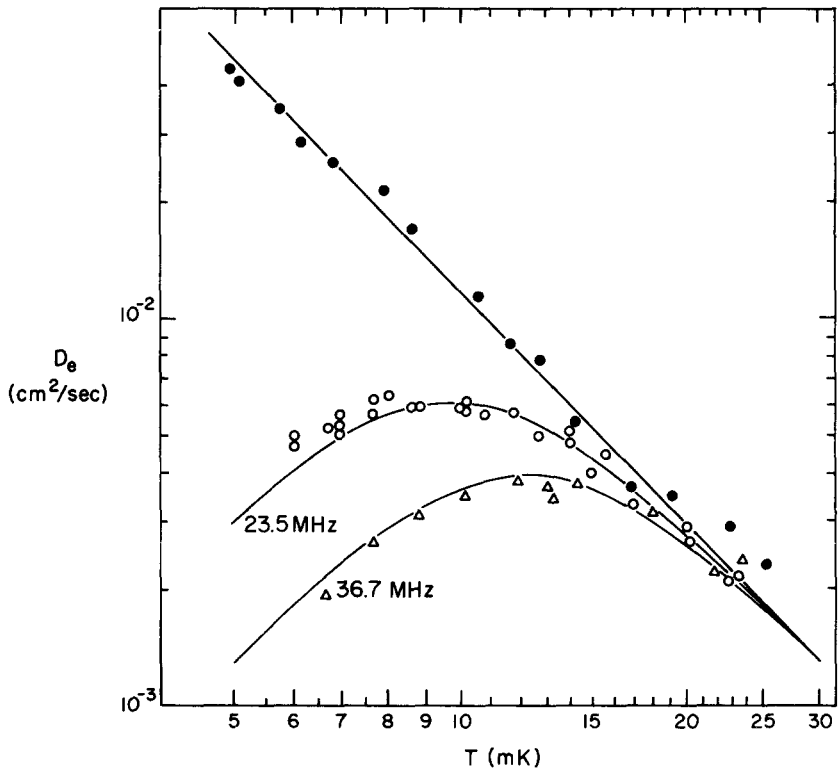


Fig. 5. Values of the effective diffusion coefficient D_e , ^3He at $P = 0$. The points with open circles and triangles were determined from the exponential attenuation of the echoes in the pulse sequence 18° - 180° -echo with various field gradients. The solid lines are calculated from Eq. (8) using $\lambda = 1.95$ and $D_0 T^2 = 1.17 \times 10^{-6} \text{ cm}^2 \cdot \text{K}^2/\text{sec}$. D_0 was determined from the data taken at 7.9 MHz in the pulse sequence 90° - 180° -echo- 180° -echo in which the exponential attenuation of the echo ratios was measured, shown with points about the upper curve.

shown are for magnetic fields with Larmor frequencies $\omega_0/2\pi$ of 23.5 and 36.7 MHz. Using the procedure just described, the value of λ obtained from these data was $\lambda = 1.95 \pm 0.1$. The solid lines in Fig. 5 were calculated from Eq. (7) using $\lambda = 1.95$ and the value of D_0 obtained from measurements in a lower field, with Larmor frequency $\omega_0/2\pi$ of 7.91 MHz. The uppermost curve is the 7.91-MHz echo ratio data. Points below 8 mK have been corrected for small departures from exponential attenuation using Leggett's Eq. (7) with $\lambda = 1.95$. The value of $D_0 T^2$ obtained in this experiment is $(1.17 \pm 0.12) \times 10^6 \text{ cm}^2 \cdot \text{K}^2 \cdot \text{sec}^{-1}$, which is somewhat lower than the values reported by Abel *et al.*²¹ of 1.36×10^{-6} . The difference in these values is within the

combined errors and could arise either from systematic errors in the spin-echo experiments or from differences in the temperature scale, most likely the former.

In Fig. 6 the echo amplitudes for various values of ϕ are analyzed using Eq. (7). The points were obtained at 6.65 mK with $\omega_0/2\pi = 36.7$ MHz and with the time between the initial pulse and the 180° pulse, $t_0/2$, equal to 3×10^{-3} sec. The points shown are for the first echo, $n = 1$. The parameter $\delta \equiv (\alpha^2/2) \sin^2 \phi / (1 + \alpha^2 \cos^2 \phi)$ was calculated using $\lambda = 1.95$ and $\tau_D T^2 = 3.67 \times 10^{-13}$ sec \cdot K 2 , as obtained from $D_0 T^2 = 1.17 \times 10^{-6}$ cm $^2 \cdot$ K 2 /sec, and using $F_0^a = -0.67$.²⁵ The echo damping measurements give excellent agreement with Eq. (7).

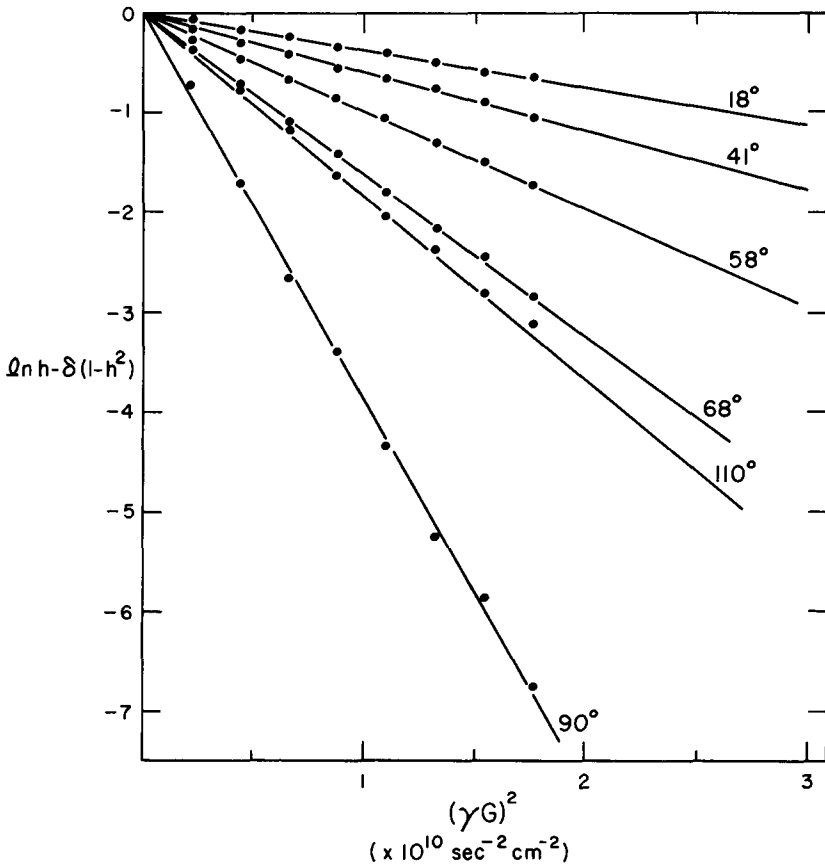


Fig. 6. The attenuation of the echo envelope at various initial tipping angles, ^3He at $P = 0$. The points are the values of $\ln h - \delta(1 - h^2)$ measured at various values of $(\gamma G)^2$ for the initial angles ϕ in the pulse sequence ϕ - 180° -echo; h is the amplitude of the echo relative to the value with $(\gamma G)^2 = 0$. The angles ϕ are indicated beside the straight lines through the points.

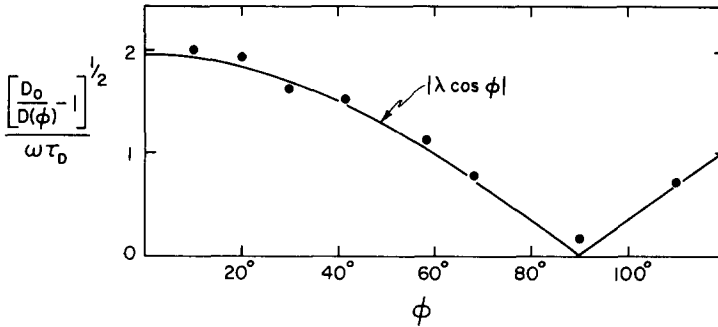


Fig. 7. The variation of D_e with ϕ . The slopes of the lines through the points in Fig. 6, and data from several other initial pulse angles, have been analyzed to determine $D_e(\phi)$. The values of D_e thus determined are plotted vs. angle in a functional form which should be proportional to $|\lambda \cos \phi|$ according to Eq. (8).

Figure 7 represents the variation in D_e with initial pulse angle for the data shown in Fig. 6, along with several other values of ϕ obtained at the same temperature and external field. The quantity $[(D_0/D(\phi)) - 1]^{1/2}/\omega_0\tau_D$, according to Eq. (7), should vary as $|\lambda \cos \phi|$, which is the curve drawn in the figure. In Fig. 7, D_0 is the average value calculated from the comparison of the data of each angle with Eq. (8). The average value of D_0 obtained in this way is 2.55×10^{-2} cm²/sec, giving $D_0T^2 = 1.13 \times 10^{-6}$. This is in good agreement with $D_0T^2 = 1.17 \times 10^{-6}$ determined from the analysis of D at 7.9 MHz. The data shown in Fig. 7 are in excellent agreement with the predicted angular dependence of D_e .

From the defining equation for λ , $\lambda = [1/(1 + F_0^a)] - \{1/[1 + (F_1^a/3)]\}$, a value of the Fermi liquid parameter F_1^a may be obtained. Using $\lambda = 1.95 \pm 0.1$, we obtain $F_1^a = -0.15 \pm 0.3$. The stated uncertainty of ± 0.1 in λ indicates the scatter in the data obtained, and does not reflect the uncertainty that exists in τ_D determined from our measurements of D_0 and from errors that might exist in Eq. (4).

3.3. ³He at 27.0 atm

After measurements at $P = 0$ were completed, the ³He pressure was raised to 27.0 atm and the measurements repeated. The resulting variation of D_e with T is shown in Fig. 8. Above 10 mK only a few points are shown, due to difficulties in obtaining thermal equilibrium. These time measurements were taken at Larmor frequencies of 7.9 and 36.7 MHz alone. As can be seen from the 36.7 MHz data, the Leggett–Rice effect is less pronounced than at $P = 0$, though not as much so as the drop in D_0 (and hence τ_D) would indicate. This shows a rise in λ with pressure.

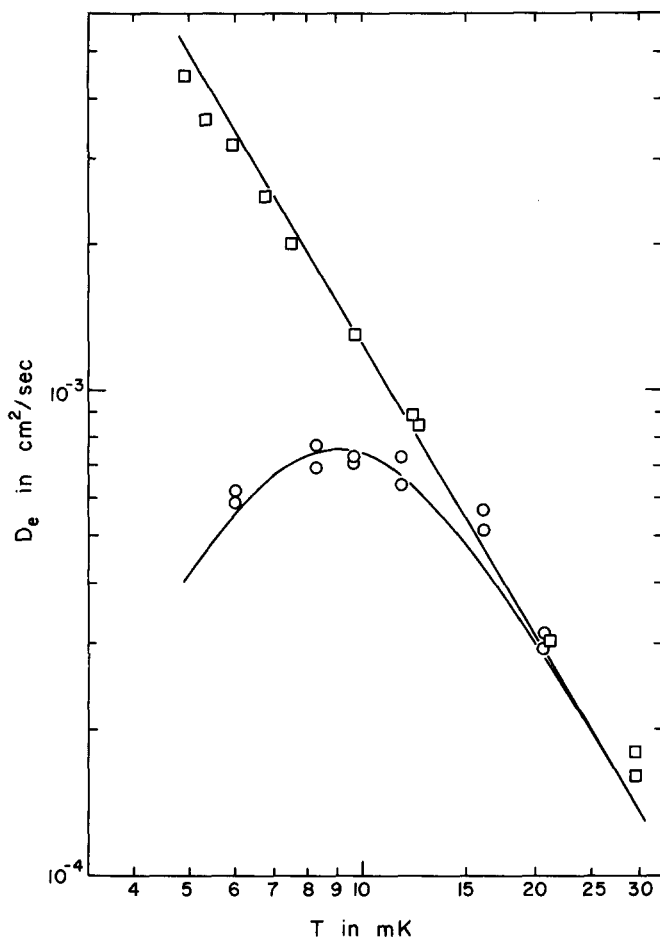


Fig. 8. Values of D_e in ^3He at 27.0 atm. The points with open circles were taken at 36.7 MHz at a tipping angle ϕ of 20° . The open squares are values of D_0 determined from echo ratios taken at 7.9 MHz; points below 8 mK have been corrected for nonexponential attenuation. The solid curve through the circles was calculated from Eq. (8) using $\lambda = 2.9$ and $D_0 T^2 = 0.125 \times 10^{-6} \text{ cm}^2 \cdot \text{K}^2/\text{sec}$.

The average λ obtained from analysis of $\phi = 20^\circ$ echo amplitudes below 10 mK is $\lambda = 2.9 \pm 0.2$. At 27.0 atm F_0^a in ^3He is -0.74 ,²⁵ giving $F_1^a = 0.2 \pm 0.6$. Apparently, F_1^a increases with pressure, in contrast to F_0^a . From the standpoint of precision it is slightly unfortunate that F_1^a is positive, since λ , the measured quantity, is much more sensitive to a large and negative F_1^a .

The value of $D_0 T^2$ determined at 7.9 MHz in this experiment is $(0.125 \pm 0.013) \times 10^{-6} \text{ cm}^2 \cdot \text{K}^2/\text{sec}$. This is again smaller than that reported by Wheatley,²³ $D_0 T^2 = 0.2 \times 10^{-6}$. The larger discrepancy is again most likely due to systematic differences in the spin-echo experiment. Our data for D_0 at 7.9 MHz in Fig. 8 are not accurately proportional to $1/T^2$; this effect has been observed previously by Wheatley,^{26,27} and is thought to arise from second-order corrections²⁸⁻³⁰ to the Fermi liquid scattering rate $1/\tau$, originating in the strong quasiparticle interactions which make liquid ^3He nearly ferromagnetic. The effect was also present to a lesser extent at $P = 0$. A $1/T^2$ fit to the data for D_0 gives $\tau_D T^2 = 0.132 \times 10^{-12} \text{ K}^2 \cdot \text{sec}$. This value was used in the subsequent analysis of D_e as a function of ϕ .

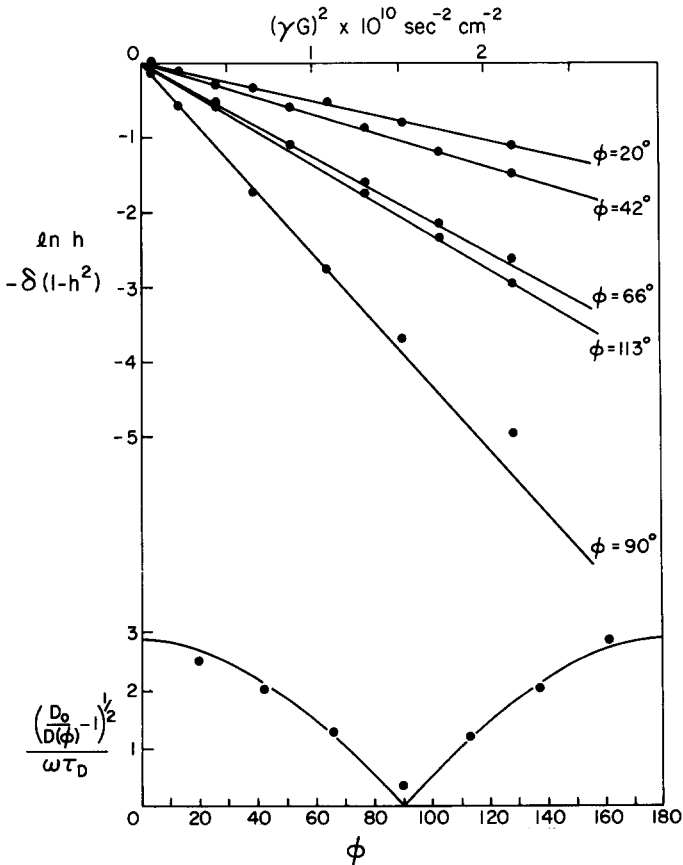


Fig. 9. Diffusion as a function of ϕ , ^3He at 27.0 atm. The upper graph shows echo attenuation as a function of gradient for various ϕ , plotted according to Eq. (7). The lower plot shows the angular dependence of the resulting values of D_e , with the theoretically expected curve $|\lambda \cos \phi|$.

The damping of echo amplitudes for various initial pulse tipping angles ϕ are analyzed in Fig. 9. Here $t_0/2$ was equal to 5 msec, reflecting the smaller value of D_0 . The points were obtained at 6.0 mK with $\omega_0/2\pi = 36.7$ MHz. The lower part of Fig. 9 shows the variation of the resulting values of D_e with ϕ , including additional values of ϕ taken at the same temperature and field. The solid curve is $|2.9 \cos \phi|$. The average value of $D_0 T^2$ obtained from these points is $(0.122 \times 10^{-6})\text{K}^2 \cdot \text{cm}^2/\text{sec}$, very close to the low-field value of 0.125×10^{-6} . Again the overall agreement with theory is very good.

3.4. ^3He - ^4He Solutions

Self-consistent measurements of the Leggett-Rice effect were obtained for one mixture, a 6.4% saturated solution at zero pressure. The Leggett-Rice effect was also observed qualitatively in a saturated solution of 8.27% at $P = 3.0$ atm, but did not yield self-consistent results. The echoes in both dilute mixtures were somewhat distorted when compared to those in pure ^3He under identical conditions, for unknown reasons. The measured values of D_e vs. T in the 6.4% solution for $\phi = 18^\circ$ are plotted in Fig. 10. Here $t_0/2 = 2$ msec for the 36.7-MHz data (open circles); $t_0/2$ for the 7.9-MHz data on the upper curve was 0.5 msec from 6 to 12 mK, and 1 msec above 10 mK, with some overlap. The value of $D_0 T^2$ obtained from the upper curve is $(70 \pm 7) \times 10^{-6} \text{cm}^2 \cdot \text{K}^2/\text{sec}$. The high-field values of D_e in Fig. 10 lie systematically above the values of D_0 at temperatures above 17 mK, for unknown reasons. The effect is not due to an error in temperature measurement, since values of D_e for $\phi = 90^\circ$ taken simultaneously with the $\phi = 18^\circ$ data shown lay on the 7.9-MHz line.

The scatter of experimental points in Fig. 10 is somewhat larger than was the case for pure ^3He . Because of this, no attempt was made to analyze individual echo amplitudes h to obtain λ . Instead, a least-squares fit to the data in Fig. 10 was used. This gives a value for α of $|\alpha| = (1.3 \pm 0.2) \times 10^{-4} \text{K}^2/T^2$. The larger error bars reflect the larger scatter in D_e .

To obtain a value of τ_D from the low-field data, a value of F_0^a must be inserted into Eq. (4). Since F_0^a in dilute mixtures has been measured to be quite small, the exact value of F_0^a used is not very critical. An approximate value of F_0^a was obtained by comparing free-induction decay amplitudes following a 90° pulse in the 6.4% solution with those in a separate 5% solution below 30 mK. These should be proportional to the Fermi liquid susceptibility.

$$\chi = m^* P_F \mu^2 / 2\pi^2 \hbar^3 k_B (1 + F_0^a).$$

Susceptibilities for the 6.4% and 5% mixtures were in the approximate ratio 1.08:1. From previously published values of F_0^a in a 5% mixture,²³ this gives $F_0^a(6.4\%) = 0.08$. While amplifier stability from one run to the

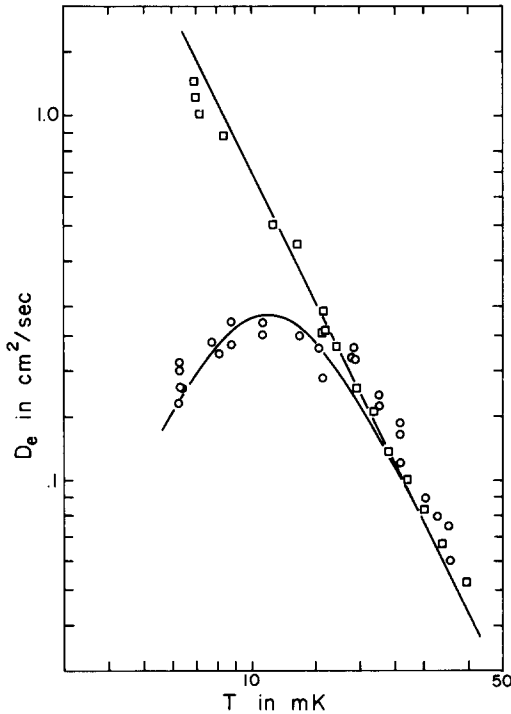


Fig. 10. Values of D_e in a 6.4% ${}^3\text{He}$ - ${}^4\text{He}$ solution. Points with open circles were taken at 36.7 MHz with a tipping angle ϕ of 18° . The open squares are values of D_0 determined at 7.9 MHz. The solid curve through the circles is the prediction of Eq. (8) using $\alpha = 1.3 \times 10^{-4} \text{ K}^2/T^2$ and $D_0 T^2 = 70 \times 10^{-6} \text{ cm}^2 \cdot \text{K}^2/\text{sec}$.

next was not good enough to give more than qualitative significance to the relative susceptibilities, it does seem to indicate (as one might intuitively suppose) that F_0^a is not very different for 5% and 6.4% mixtures.

Using $F_0^a = 0.08$ to evaluate τ_D gives $\tau_D T^2 = (2.24 \times 10^{-11}) \text{ sec} \cdot \text{K}^2$, resulting in $|\lambda| = (0.025 \pm 0.005)$. Due to the small size of F_0^a , it is not possible to say with any assurance whether λ is positive or negative. Because of this, and also because of the large uncertainty in F_0^a , no quantitative conclusion regarding F_1^a can be made. However, an assumption of $F_0^a = 0.08$ leads to $F_1^a \approx +0.3$ for $\lambda > 0$, and $F_1^a \approx +0.15$ for $\lambda < 0$. Since particle interactions in dilute ${}^3\text{He}$ - ${}^4\text{He}$ mixtures are known to be weak, it might be argued from these numbers that λ is most likely negative, and F_1^a positive.

Using the least-squares value of α , the angular dependence of D_e was then analyzed using Eq. (7). Figure 11 shows the damping of echo amplitudes

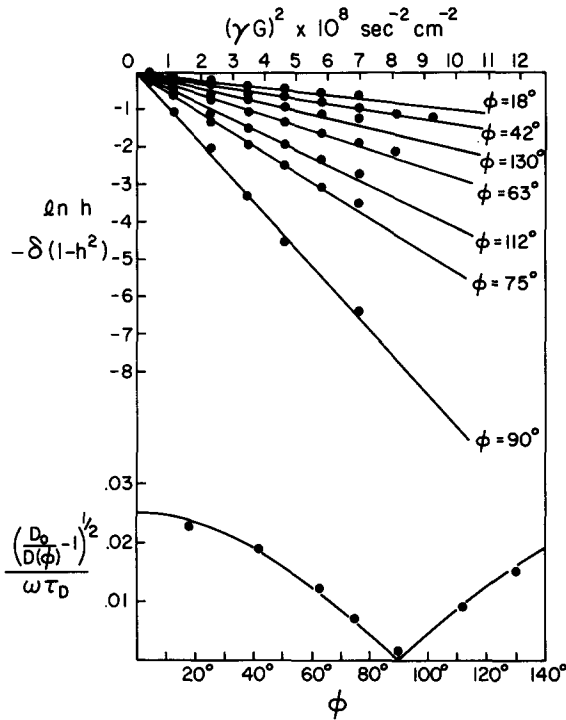


Fig. 11. Diffusion as a function of ϕ , 6.4% solution. The upper graph is the echo attenuation plotted according to Eq. (7) as a function of gradient. The resulting values of $D_e(\phi)$ are plotted below with the theoretical prediction $|\lambda \cos \phi|$ for $\lambda = 0.025$.

h for various ϕ in the 6.4% mixture. The points shown were taken at 6.4 mK. The mean value of $D_0 T^2$ determined from the data of Fig. 11 is $73 \times 10^{-6} \text{ cm}^2 \cdot \text{K}^2/\text{sec}$, agreeing very well with the value obtained at 7.9 MHz, $D_0 T^2 = 70 \times 10^{-6}$. The lower part of Fig. 11 shows the variation of D_e with ϕ determined from the slopes of the lines above. Again the solid curve is $|\lambda \cos \phi|$ with $\lambda = 0.025$. While agreement with theory is not as precise as in ^3He , it is still satisfactory.

As mentioned previously, the Leggett–Rice effect was observed qualitatively in a saturated solution of 8.27% at 3.0 atm. The limiting concentration is taken from the work of Watson *et al.*^{31,32} While quantitative results could not be obtained at high field, reliable data for D_0 was obtained at 7.9 MHz. The low-field data are shown in Fig. 12. No corrections for the Leggett–Rice effect at low temperature have been made. This would tend to raise the points

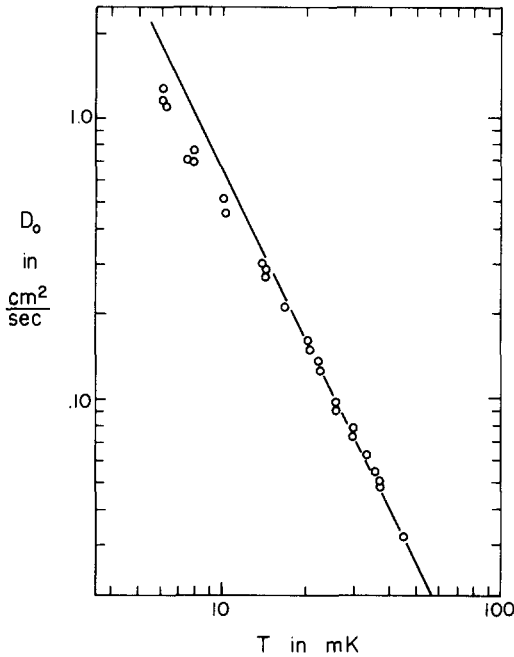


Fig. 12. D_0 as a function of T , 8.27% saturated solution at 3.0 atm. No corrections for the Leggett-Rice effect have been made; this would tend to raise the values at the low-temperature end.

at the low-temperature end of the curve. $D_0 T^2$ for this mixture was measured to be $(66 \pm 7) \times 10^{-6} \text{ cm}^2 \cdot \text{K}^2/\text{sec}$, slightly less than the value for 6.4%.

4. CONTINUOUS WAVE NMR APPARATUS AND RESULTS

A cw NMR measurement of $\chi(k, \omega)$, the Fermi liquid dynamic susceptibility, would be valuable for several reasons. Apart from providing a second and somewhat more direct observation of spin waves in liquid ^3He systems, an observation of the spin-wave poles in $\chi(k, \omega)$ would directly measure the imaginary part of the complex spin diffusion coefficient D^* , including the sign of λ . In this respect the pulsed and cw experiments are complementary, since the pulsed measurements provide only the real part of D^* .

For these reasons continuous wave NMR measurements using a variety of coils were made in an effort to detect single spin-wave modes. The different chambers were all designed to permit a direct measurement of the dynamic

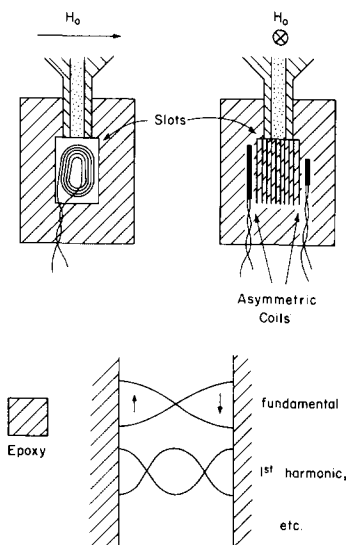


Fig. 13. Cavity resonator for spin waves. Schematic views at the top show slots in the epoxy chamber sandwiched between flat, asymmetrical Helmholtz coils. Below is shown a magnified slot containing ^3He , with the expected standing-wave patterns.

susceptibility $\chi''(k, \omega)$ through resonant absorption. One type of chamber was designed as a cavity resonator, shown in the upper part of Fig. 13. Asymmetrical Helmholtz coils cast in an epoxy block provide a very inhomogeneous rf magnetic field to excite the spin waves. Between the two coils are slots in the epoxy 0.025 mm across. These were produced by casting parallel strips of 0.025 mm copper foil in the epoxy, counterboring the ends of the piece to expose the copper, and then etching the whole piece for about a month in a concentrated solution of ferric chloride. After cleaning with dilute HCl, clear gaps are left behind in the epoxy. The epoxy used for this construction was Stycast 1269A, chosen because its low viscosity when heated enables it to fill the spaces between copper sheets by capillary action. Changes in the gap spacing through flexure were minimized by etching small slots approximately 3 mm long and spaced 1.5 mm apart in the copper strips before casting. After the final etching, small pillars of epoxy were left between the gap walls. Microscope examination showed the gaps to be uniform to $\pm 5\%$ both before and after the experiment.

The idea behind the design is that standing spin-wave modes driven by the inhomogeneous rf field will resonate in the gaps at a particular frequency ω , providing a direct verification of the spin-wave spectrum through measurement of ω and knowledge of k through the gap spacing. In the absence of magnetic cavity walls, the waves will interfere to form antinodes at the walls, as depicted in the lower part of Fig. 13. The net magnetization in each mode is zero, hence the need for a spatially inhomogeneous exciting field.

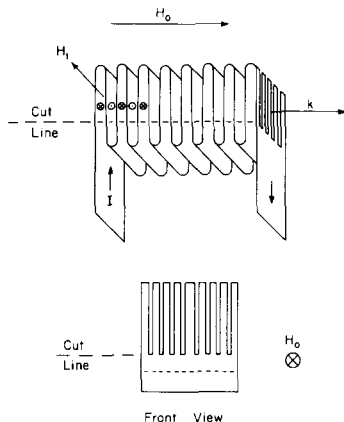


Fig. 14. *z*-folded spin wave generator. This simplified drawing shows the path of the current I and the orientation of the external field H_0 . The periodic rf magnetic field H_1 should excite spin waves of wave vector k at the boundaries of the cuts.

A second type of chamber utilized a spatially varying rf field with a uniform periodicity or finite k . The field is set up by an array of current sheets folded back on one another with the proper spacing in a *z*-folded array, as shown in Fig. 14. The idea for the design was suggested to us by Professor W. Gilbert Clark of UCLA. The spin waves should propagate perpendicular to the sheets in the slots, parallel to k . The chamber was made from copper foil folded accordionlike with 0.028-mm cigarette paper between folds for electrical insulation. This was cast in Stycast 1269A while compressed together with teflon blocks. After curing, 8 slots were cut partway through the piece in planes perpendicular to the fold axis, to provide adequate filling factor. The cuts were made with a string saw of the sort used for sectioning crystals, using a serrated metal guide to keep the blade from wandering. When finished the chamber measured 5.7 mm wide, 2.82 mm thick, and 1.27 cm long, and the calculated filling factor was approximately 10%. The measured k of the chamber was 840 cm^{-1} .

Both chambers were installed in the same apparatus used for the spin diffusion measurements. The cavity resonator replaced the pulsed NMR coil, and the *z*-folded chamber was placed in a counterbored cavity in the tail-piece above it, just below the thermometer.

The circuit for the cw measurements utilizes a frequency-swept oscillator and a standard Rollin circuit. A block diagram is shown in Fig. 15. The voltage ramp from the digital signal averager, a Fabri-Tek model 1072, sweeps the frequency through the region of interest, and resonant absorption proportional to $\chi''(k_n, \omega)$ should take place, where $k_n = nk_0$ corresponds to the n th harmonic of k_0 . The absorption signal is amplified, detected, and averaged over many sweeps by the signal averager.

Since liquid ^3He at $P = 0$ showed the maximum Leggett effect in the previous diffusion measurements, it was chosen for the cw experiment. The

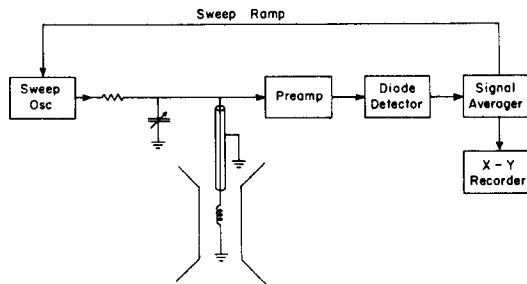


Fig. 15. Continuous wave NMR electronics. The frequency of the cw oscillator is swept through the region containing the Larmor resonance by the signal averager. The resulting nuclear absorption signal is detected and averaged over many sweeps to improve the signal-to-noise ratio.

observed absorption $\chi''(k, \omega)$ for the two chambers is shown in Fig. 16. Both were taken at a temperature of 7 mK in a field of 13.44 kG, corresponding to $\omega_0/2\pi = 43.6$ MHz. The upper trace is from the z-folded chamber. This device has an inherently low Q , so the signal-to-noise ratio is quite poor, as can be seen. Still, at this temperature and field, the pole of $\chi''(k, \omega)$ for $k =$

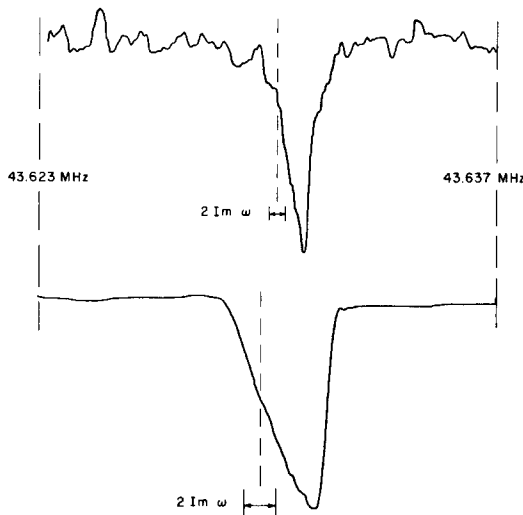


Fig. 16. Observed $\chi''(k, \omega)$ at $T = 7$ mK in ^3He . The upper trace is from the z-folded chamber, the lower from the cavity resonator. Theoretically expected splittings for the first sideband in both chambers are shown by the vertical dashed lines, along with collisional line widths $2 \text{Im}\omega$.

840 cm^{-1} should be roughly comparable to the Larmor resonance in magnitude, and would be visible either as a broadening of the Larmor resonance on the low-field side or as a distinct sideband. Neither was observed. The theoretically expected position of the fundamental sideband is shown by the vertical dashed line, calculated using Eq. (1) with $\lambda = 1.95$, $k = 840 \text{ cm}^{-1}$, and $D_0 T^2 = 1.17 \times 10^{-6} \text{ cm}^2 \cdot \text{K}^2/\text{sec}$. The collisional line width $2 \text{Im } \omega$, also calculated from Eq. (1), is shown for comparison with the Larmor line width. The lower part of Fig. 16 is the trace from the cavity resonator. As can be seen, the signal-to-noise ratio was much better for this chamber. No evidence of a spin-wave pole was observed here either. The expected sideband splitting and line width shown in the figure were calculated as before using $k = 1240 \text{ cm}^{-1}$. The asymmetrical Larmor resonance is a function of the coil geometry and was not temperature dependent. At a temperature of 40 mK, both traces were unchanged.

The failure to observe spin-wave poles in $\chi''(k, \omega)$ is most likely traceable to inefficient exciters. Apparently the rf magnetic field produced by the cavity resonator coils is not sufficiently inhomogeneous to couple strongly to the spin waves. The field produced by the z-folded chamber should be sufficiently inhomogeneous, but the folded copper sheets may be shorted out by shunt capacitance, and filling factor may not be adequate.

5. CONCLUSIONS

In summary, the magnetic effects predicted by Leggett and Rice for Fermi liquids in the collisionless regime have been verified. Within experimental scatter, our results accurately obey Leggett's basic equation (7), and provide direct evidence for the existence of spin waves and undamped spin currents in liquid ^3He systems. These results, taken together with those of Ref. 6, suggest that spin-wave phenomena are a universal characteristic of any Fermi liquid. This would not seem to be the case for zero sound, where the degree of freedom provided by the magnetic field is missing.

It should be pointed out that measurements of spin diffusion coefficients are particularly subject to systematic errors, since errors in gradient enter as the square and errors in time as the cube. Furthermore, in Fermi liquids errors in T enter as the square. For this reason the values of the Fermi liquid parameter λ derived from these measurements should be regarded as rather tentative and subject to correction from further experiments.

In this connection it would be interesting to explore the diffusion-dependent effective Larmor line width $1/T_2$ as a function of magnetic field and temperature. According to the results of Platzman and Wolff, the real part of D^* contributes to the Larmor line width as described by Eq. (1). In the collisionless regime T_2 may conceivably show a temperature dependence

similar to that of $1/D_{\text{eff}}$, showing a minimum at the same temperature where D_{eff} shows a maximum. The effective T_2 could be easily measured using Carr–Purcell²¹ techniques, and would be free of errors due to gradient calibration. Conceivably the effective T_2 would depend on ϕ , the initial pulse angle.

With regard to the cw measurements of $\chi(k, \omega)$, it seems that spin waves are rather difficult to excite using rf devices geometrically shaped to couple to the wave. It may be that a more efficient technique would be a variation of the mechanism pictured in Fig. 2, using a periodically varying magnetization in the ^3He itself to excite the waves. Such a magnetization might be produced by using a pulsed gradient.

ACKNOWLEDGMENT

We are most grateful to Professor David Mermin for many conversations about this topic.

REFERENCES

1. L. D. Landau, *Soviet Phys.—JETP* **3**, 920 (1957); **5**, 101 (1957).
2. W. R. Abel, A. C. Anderson, and J. C. Wheatley, *Phys. Rev. Letters* **17**, 74 (1966).
3. V. P. Silin, *Soviet Phys.—JETP* **6**, 945 (1958).
4. P. M. Platzman and P. A. Wolff, *Phys. Rev. Letters* **18**, 280 (1967).
5. D. Hone, *Phys. Rev.* **121**, 669 (1961).
6. S. Schultz and G. Dunifer, *Phys. Rev. Letters* **18**, 283 (1967).
7. A. J. Leggett and M. J. Rice, *Phys. Rev. Letters* **20**, 586; **21**, 506 (1968).
8. H. C. Torrey, *Phys. Rev.* **104**, 563 (1956).
9. A. J. Leggett, *Proc. 11th Conf. Low Temp. Physics* (St. Andrews, Scotland, 1968), Vol. 1, p. 400.
10. A. J. Leggett, *J. Phys. C* **3**, 448 (1970).
11. S. Doniach, *Phys. Rev.* **177**, 336 (1969).
12. L. R. Corruccini, D. D. Osheroff, D. M. Lee, and R. C. Richardson, *Phys. Rev. Letters* **27**, 650 (1971).
13. J. C. Wheatley, O. E. Vilches, and W. R. Abel, *Physics* **4**, 1 (1968).
14. J. R. Sites, D. D. Osheroff, R. C. Richardson, and D. M. Lee, *Phys. Rev. Letters* **23**, 836 (1969).
15. R. T. Johnson and J. C. Wheatley, *J. Low Temp. Phys.* **2**, 423 (1970).
16. A. C. Anderson, J. I. Connolly, O. E. Vilches, and J. C. Wheatley, *Phys. Rev.* **147**, 86 (1966).
17. D. D. Osheroff and D. M. Lee, to be published.
18. For a discussion of this technique see R. A. Scribner and E. D. Adams, *Fifth Symposium on Temperature*, Washington, D.C. (National Bureau of Standards, 1971), to be published.
19. W. G. Clark, *Rev. Sci. Instr.* **35**, 316 (1964).
20. D. S. Miyoshi, thesis, Cornell University, 1969, unpublished.
21. W. R. Abel, A. C. Anderson, W. C. Black, and J. C. Wheatley, *Physics* **1**, 337 (1965).
22. H. Y. Carr and E. M. Purcell, *Phys. Rev.* **94**, 630 (1954).
23. J. C. Wheatley, in *Quantum Fluids*, D. F. Brewer, ed. (North-Holland, Amsterdam, 1966), p. 206.
24. A. C. Anderson, D. O. Edwards, W. R. Roach, R. E. Sarwinski, and J. C. Wheatley, *Phys. Rev. Letters* **17**, 367 (1966).
25. H. Ramm, P. Pedroni, J. R. Thompson, and H. Meyer, *J. Low Temp. Phys.* **2**, 539 (1970).

26. J. C. Wheatley, *Phys. Rev.* **165**, 304 (1968).
27. J. C. Wheatley, in *Progress in Low Temperature Physics*, C. J. Gorter, ed. (North-Holland, Amsterdam, 1970), Vol. 6, p. 80.
28. M. J. Rice, *Phys. Rev.* **162**, 189 (1967).
29. V. J. Emery, *Phys. Rev.* **170**, 205 (1968).
30. C. J. Pethick, *Phys. Letters* **27A**, 219 (1968); *Phys. Rev.* **177**, 391 (1969).
31. G. E. Watson, J. D. Reppy, and R. C. Richardson, *Phys. Rev.* **188**, 384 (1969).
32. G. E. Watson, thesis, Cornell University, 1969, unpublished.